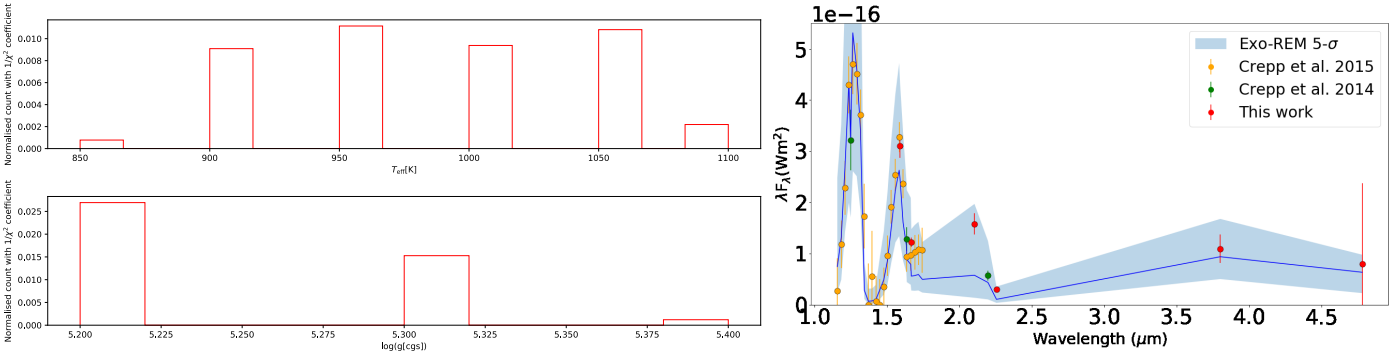

Fig. 10. *Left*: histograms of the effective temperature (*top*) and surface gravity (*bottom*) of the models from Exo-REM, reproducing the data, without cloud covering all metallicity values (see text). The number of count is normalized using the invert of the χ^2. *Right*: comparison of the best-fit model spectra (dark blue line: best fit, light blue area: 5σ envelope) and of the mesured SED (colored data points).

Table 7. Retrieved HD 19467B's atmospheric parameters.

Model name	$T_{\rm eff-cloudy}$ (K)	$T_{\rm eff-cloud-free}$ (K)	$\log g$ (dex)	[Fe/H] (dex)	$f_{\rm sed}$	CF	R_p (R_J)	M_p (M_J)	$\chi^2_{\rm min}$
Exo-REM-cloud free	–	975 ± 125	5.2 ± 0.1	UC	–	(1.0)	–	–	231
petitCODE-cloud free	–	1186^{+24}_{-27}	$5.61^{+0.06}_{-0.05}$	$0.18^{+0.12}_{-0.11}$	–	(0.0)	$0.59^{+0.03}_{-0.03}$	57^{+7}_{-4}	103.3
petitCODE-cloudy	1044^{+12}_{-18}	–	$5.33^{+0.05}_{-0.05}$	$-0.05^{+0.07}_{-0.07}$	$1.02^{+0.39}_{-0.28}$	(1.0)	$0.84^{+0.04}_{-0.02}$	63^{+6}_{-7}	101.3
petitCODE-patchy	932^{+66}_{-63}	1291^{+99}_{-89}	$5.34^{+0.08}_{-0.09}$	$0.03^{+0.08}_{-0.08}$	$1.20^{+0.79}_{-0.46}$	$0.79^{+0.10}_{-0.15}$	$0.83^{+0.09}_{-0.06}$	60^{+7}_{-6}	86.6
Morley 2012	928^{+39}_{-42}	–	$5.20^{+0.09}_{-0.10}$	(0.0)	$4.07^{+0.41}_{-0.49}$	(1.0)	$0.99^{+0.10}_{-0.09}$	63^{+6}_{-7}	129.7

Notes. Values given in parenthesis are priors or assumptions and are not retrieved (see text). UC: unconstrained.

the radius to decrease or increase to fit in this range. The only rule was to stay in the confidence interval (5σ).

In these χ^2 maps, we only kept the results that reproduced the data at less than 5-σ, with a radius solution between 0.7–1.3 R_J and a mass solution between 52–72 M_J (based on the system's dynamics). Although the adopted mass prior includes smaller values than the actual constraints from the orbital fit (Sect. 4.3), the choice of the bounds has a negligible effect on the derivation of the atmospheric parameters. The radius prior has a larger effect. The models fit the data only without clouds (the best fit with clouds is out at more than 10σ). We do not observe any clues about the metallicity. Figure 10 shows the histograms of the $T_{\rm eff}$ and $\log g$ reproducing the data and the comparison of the best-fit spectra to the measured SED. The count of the histograms is normalized using the invert of the χ^2 as a coefficient to highlight the best-fit cases. The inferred $T_{\rm eff}$ is 975 ± 125 K, the inferred $\log(g[\rm cgs]) = 5.2 \pm 0.1$ (Table 7). We also provide in Table 7 the χ^2 values associated with the best-fit solution computed according to the definition of Baudino et al. (2015).

5.2.2. petitCODE models

As the second approach, we used petitCODE (Mollière et al. 2015, 2017) to calculate a grid of self-consistent models; assuming both cloud-free and cloudy atmospheres. The characteristics of these models are summarized in Table 6. For the cloudy models, the species included are Na_2S and KCl. The free parameters in the cloud-free models are the effective temperature, the surface gravity, and the metallicity. For the cloudy models, the sedimentation factor ($f_{\rm sed}$) is also taken into account as a free parameter.

We performed Bayesian analysis using the `emcee` tool (Foreman-Mackey et al. 2013) to explore the atmospheric properties of HD 19467B with the petitCODE models. We considered the statistical treatment of observational uncertainties and explored any underestimation of these uncertainties through a Gaussian Process. Uninformative priors were also assumed for the initialization of the walkers in the MCMC process.

Firstly, we fit the data with cloud-free models. Figure 11 shows the results and the corner plot of the retrieved parameters. The retrieved properties of HD 19467B are as follows, assuming a cloud-free atmosphere (Table 7): an effective temperature of 1186^{+24}_{-27} K, a surface gravity of $5.61^{+0.06}_{-0.05}$ dex, and a metallicity of $0.18^{+0.12}_{-0.11}$ dex. The radius is $0.59^{+0.03}_{-0.03}$ R_J and the mass is 57^{+7}_{-4} M_J. As discussed, cloud-free models could explain the SED, although tentatively. The photometric points, in particular at 1.633 μm, 2.255 μm, and 3.8 μm, disagree with the best-fit model, with the first two by at least 3σ (dotted lines in the bottom panel of Fig. 11). In addition, the inferred radius of the companion is significantly smaller than the expected radius from the evolutionary tracks (0.8 R_J). We therefore examined cloudy models to improve the fit.

Secondly, we fit the data with cloudy models. We assumed $52 < M_p < 72$ M_J and $0.7 < R_p < 1.3$ R_J as priors. Figure 12 shows the fitted models to the data and the corner plot of the retrieved parameters. The retrieved atmospheric properties are as follows (Table 7): $T_{\rm eff} = 1044^{+12}_{-18}$ K, $\log g = 5.33^{+0.05}_{-0.05}$ dex, and $[\rm Fe/H] = -0.05^{+0.07}_{-0.07}$ dex, all have values less than their counterparts when fitting with petitCODE cloud-free models. This behavior can be explained by the prior used for the companion radius, which excludes radii smaller than 0.7 R_J. The best-fit value for $\log(f_{\rm sed})$ is $0.01^{+0.14}_{-0.14}$, which corresponds to a

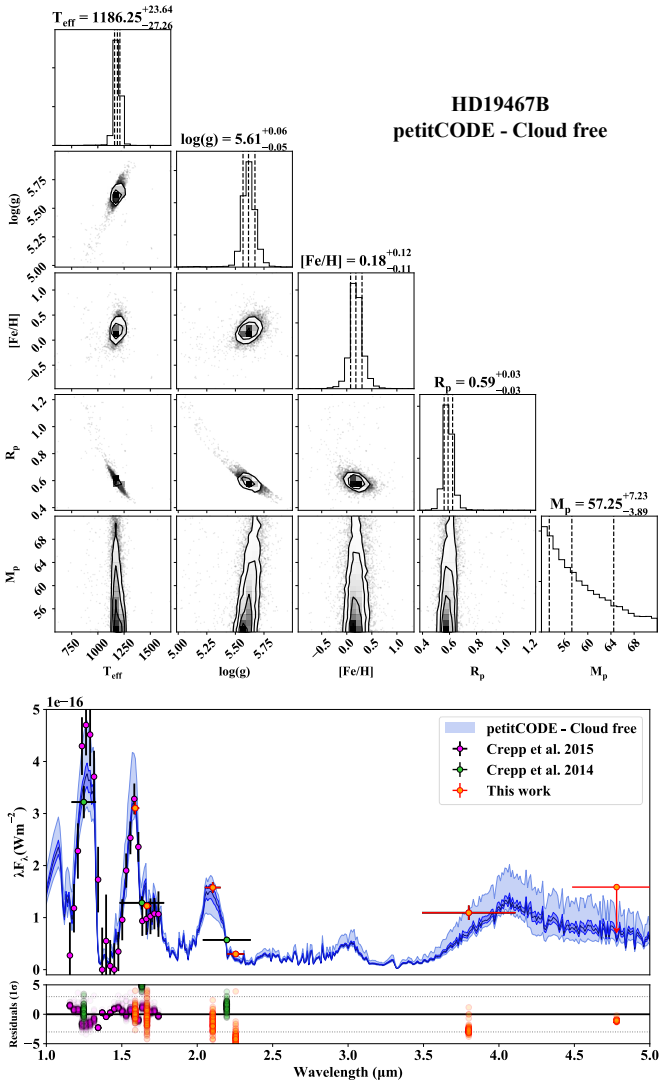

Fig. 11. Atmospheric fitting of HD 19467B with petitCODE cloud-free models. *Top panel*: corner plot of the retrieved atmospheric parameters. *Bottom panel*: comparison of the best-fit model spectra and of the measured SED (colored data points). For the model spectra, the dark blue area corresponds to the region of the posteriors between the 16 and 84% quantiles and the light blue area to the region between the 1 and 99% quantiles.

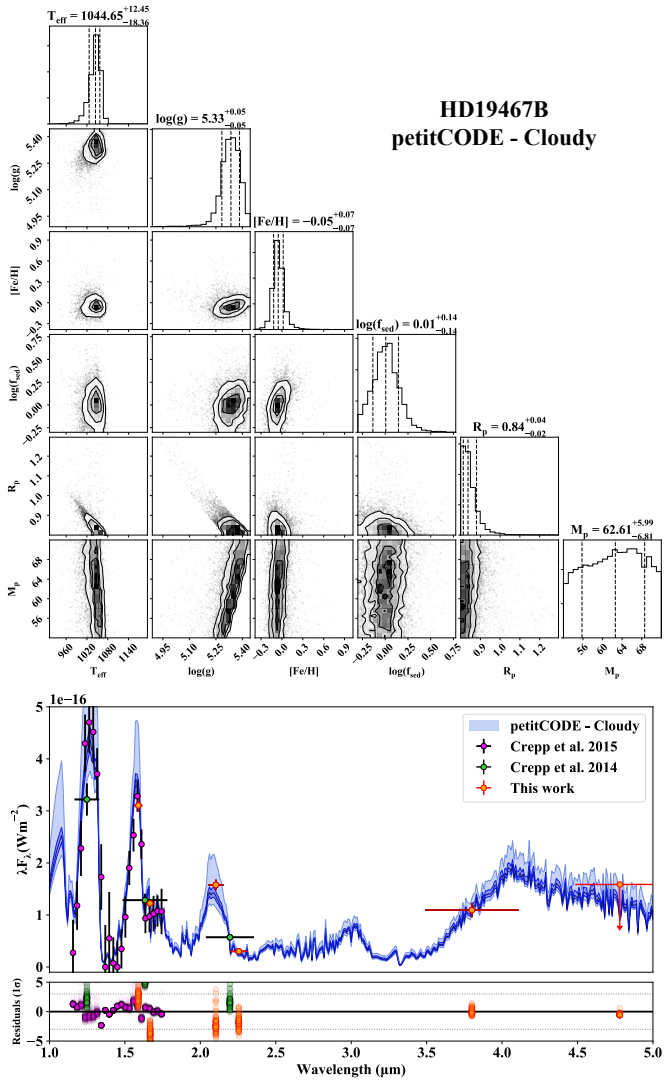

Fig. 12. Atmospheric fitting of HD 19467B with petitCODE cloudy models. For the radius posterior, values smaller than 0.78 R_J are disfavored.

sedimentation factor of 1.0. This suggests that an active removal of the clouds is required for the clouds to fit the observations. We note that the cloud species considered in these petitCODE cloudy models are Na_2S and KCl, which both have a relatively low evaporation temperatures at typical photospheric pressures (i.e., around 1000 K at 1 bar). The fitted temperature of ∼1050 K suggests that these species have a reduced contribution to the cloud opacities; supporting an optically thin atmosphere hypothesis. The retrieved radius is $0.84^{+0.04}_{-0.02}$ R_J and the retrieved mass is 63^{+6}_{-7} M_J. While the best fitted petitCODE's cloudy models agree with most data points within 3σ, fitting the photometric point at 1.633 μm demands relaxation of the model.

Thirdly, we examined the idea of a patchy atmosphere for HD 19467B, following the method in Samland et al. (2017). In this approach, we took one cloudy model and one cloud-free model and combined them linearly as below:

$$F_{\rm patchy} = CF \cdot F_{\rm cloudy} + (1 - CF) F_{\rm cloud-free} \quad (1)$$

where $F_{\rm cloudy}$ and $F_{\rm cloud-free}$ are the flux of cloudy and cloud-free models. CF is the cloud fraction, which has a value ranging from 0 (no cloud) to 1 (fully cloudy). We also imposed a prior on the temperature of the patches, where the temperature of the cloudy parts was assumed to be smaller than the temperature of the cloud-free parts, $T_{\rm cloudy} < T_{\rm cloud-free}$. The surface gravity and metallicity of these patches were assumed to be the same. Figure 13 shows the best-fit results and retrieved parameters assuming a patchy atmosphere. While taking this approach does not improve the fit significantly, the radius of the companion is constrained. The retrieved atmospheric properties are $T_{\rm eff-cloudy} = 932^{+66}_{-63}$ K, $T_{\rm eff-cloud-free} = 1291^{+99}_{-89}$ K, $\log g = 5.34^{+0.08}_{-0.09}$ dex, [Fe/H] $= 0.03^{+0.08}_{-0.08}$ dex, and $\log(f_{\rm sed}) = 0.08^{+0.22}_{-0.21}$ (Table 7). The cloudy temperature agrees with the retrieved temperature by Crepp et al. (2015) and the cloud-free temperature would agree better with the expectations given the age and dynamical mass (Sect. 6). A cloud fraction of CF ∼ 0.8 ± 0.1 hints for an atmosphere to be mostly covered by clouds. Given the cloud-free and cloudy temperatures and the cloud fraction, the global temperature is 1042^{+77}_{-71} K. Nevertheless, the relatively high $f_{\rm sed}$ and low evaporation temperatures of the cloud species considered in the cloudy models, as discussed

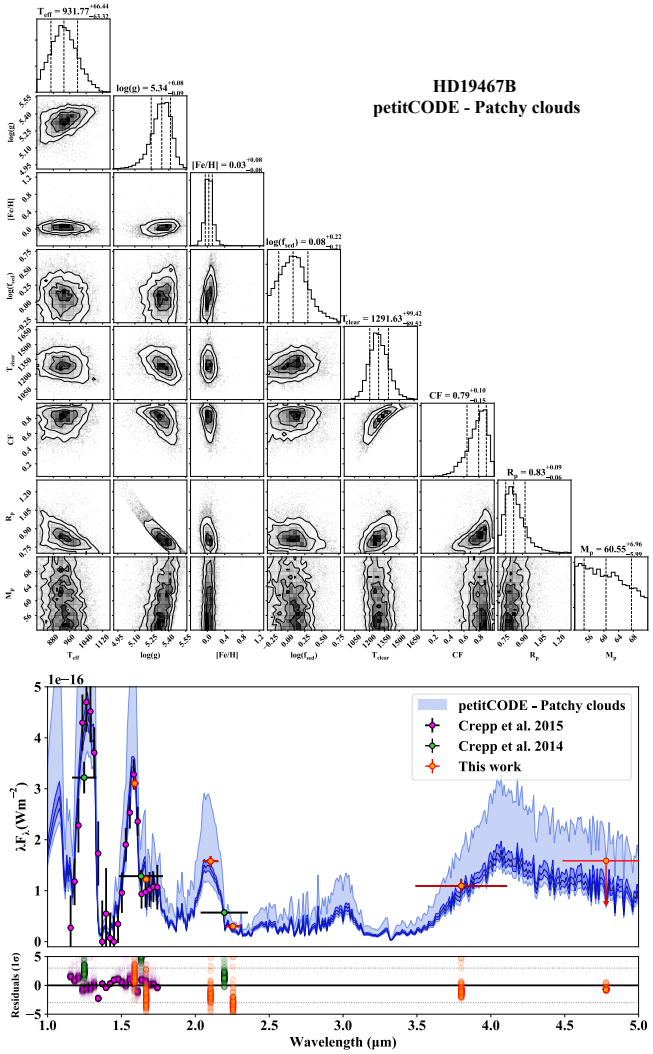

Fig. 13. Atmospheric fitting of HD 19467B with petitCODE patchy cloudy models with temperature constraints (see text).

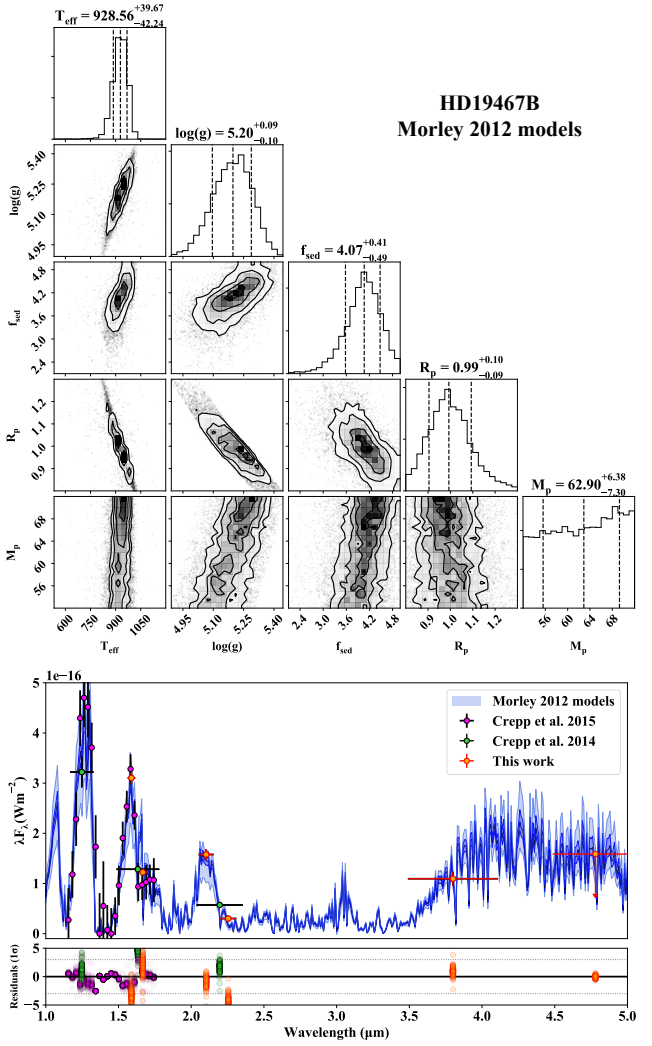

Fig. 14. Atmospheric fitting of HD 19467B with the models of Morley et al. (2012).

above, call for an optically thin cloud layer. The retrieved radius is $0.83^{+0.09}_{-0.06}$ R_J and the retrieved mass is 60^{+7}_{-6} M_J. The patchy model constrains the radius of the companion well and in agreement with the evolutionary tracks.

5.2.3. Morley 2012 models

We also fit the SED using the grid of models in Morley et al. (2012). The properties of their grid are summarized in Table 6. The cloud species included are Na_2S, KCl, ZnS, MnS, and Cr. We note that they assume some additional cloud species in the models. This results in an abundance of cloud opacities in colder regimes, where more condensates can form to add to the opacity contribution of clouds. A higher retrieved sedimentation factor, $4.07^{+0.41}_{-0.49}$, is likely a consequence of this treatment of cloud species (Fig. 14 and Table 7). Other retrieved atmospheric parameters are $T_{\rm eff} = 928^{+39}_{-42}$ K and $\log g = 5.20^{+0.09}_{-0.10}$ dex. The radius is $0.99^{+0.10}_{-0.09}$ R_J and the mass is 63^{+6}_{-7} M_J. While the radius is constrained, the value is larger than the expected value from the evolutionary tracks (~0.8 R_J).

5.2.4. Conclusion and remarks

We conclude that the SED of HD 19467B is consistent with a patchy atmosphere mostly covered by thin clouds. A summary of the retrieved parameters is given in Table 7. It is worth highlighting the relative consistency of the retrieved surface gravity in all the tested atmospheric models, which suggests an object with a high surface gravity (greater than 5.1 dex). A solar metallicity is consistent with all analyses (~0.0, for the Exo-REM and petitCODE models). All our retrieved surface gravities are at the high end or larger than the surface gravities of 4.21–5.31 dex inferred by Crepp et al. (2015) using BT-Settl models.

The effective temperatures retrieved for the fits of the models of Morley et al. (2012) and of the cloudless Exo-REM models agree well with the expectations from the empirical relations of Filippazzo et al. (2015) for field dwarfs given its measured absolute magnitude in H band (~875–975 K, see their Fig. 16). The global temperature inferred from the petitCODE patchy model fit (971–1119 K) is slightly higher by ~1σ. The expected range of effective temperatures from Filippazzo et al. (2015) given the measured spectral type is much wider (~840–1185 K, see their Fig. 15). All our atmospheric fits agree with it. Finally, we note that given the age and dynamical mass of the companion, evolutionary models (Sect. 6) predict surface gravities higher than 5.3 dex. Only the atmospheric fits with the petitCODE models retrieve such large values.

In all the atmospheric fits, the H broad-band photometric point reported by Crepp et al. (2014) is off by at least ~3σ.

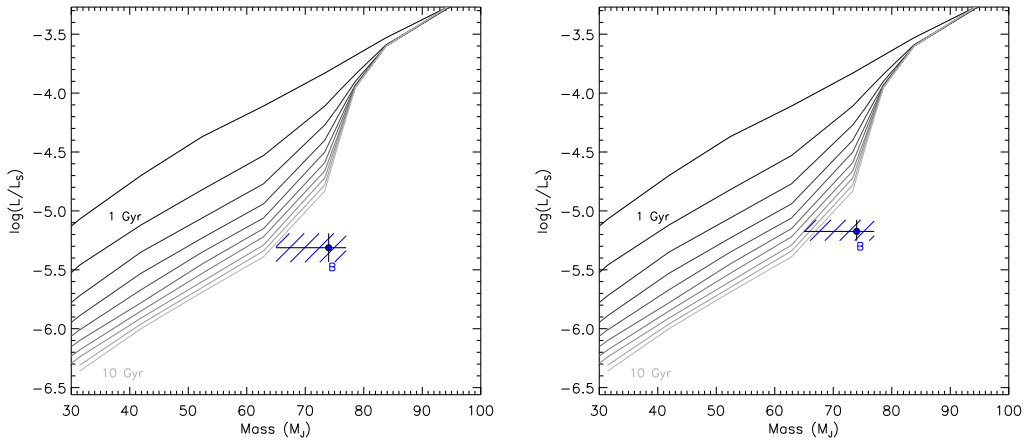

Fig. 15. Bolometric luminosity of HD 19467B computed using the NIRC2 photometry in the K_s band (*left*) and in the J band (*right*) and the relations of Filippazzo et al. (2015) for field dwarfs as a function of the mass estimated from the orbital fit and the theoretical hydrogen-burning mass limit (see text). For comparison, the model isochrones of Baraffe et al. (2003) are indicated.

Mesa et al. (2020) estimated from a long-slit spectrum an absolute photometry in the H band of 15.84 ± 0.08 mag assuming the distance derived from the *Gaia* parallax. This is fainter by $\sim 3.4\sigma$ than the photometry of 15.37 ± 0.11 mag derived in Sect. 6 from the apparent magnitude in Crepp et al. (2014). The fainter H-band magnitude found by Mesa et al. (2020) implies a redder H-L' color by 0.47 mag in the bottom-right panel of Fig. 9. It points toward lower effective temperatures of ~800–890 K using the empirical relation of Filippazzo et al. (2015). Our absolute magnitude in the J band of 15.08 ± 0.11 mag recomputed from the apparent magnitude in Crepp et al. (2014) agrees with the value of 15.13 ± 0.02 mag reported by Mesa et al. (2020).

6. Comparison of the properties of HD 19467B to model predictions

Regarding a possible formation mechanism for HD 19467B, the mass ratio derived in Sect. 4.4 (0.065–0.086 at 68%) is large and challenging to explain in a disk gravitational instability scenario (Boss 1997) without additional mechanisms (non-in situ formation with migration, mass accretion after formation). This would support a stellar-like (or stellar binary-like) formation scenario for the companion.

Figure 15 compares the bolometric luminosity and mass of HD 19467B to the model isochrones from Baraffe et al. (2003). To derive the bolometric luminosities, we used the model relations for field dwarfs of Filippazzo et al. (2015), a bolometric luminosity for the Sun of 4.74 dex (Prša et al. 2016), the absolute magnitudes in the J and K_s bands in Crepp et al. (2014) corrected for the new distance estimate from *Gaia* ($M_J = 15.08 \pm 0.11$ mag, $M_H = 15.37 \pm 0.11$ mag, $M_{K_s} = 15.44 \pm 0.09$ mag), and the spectral type of T5.5 ± 1.0 in Crepp et al. (2015). We find $\log(L/L_\odot) = -5.17^{+0.10}_{-0.08}$ dex from the J-band magnitude and $\log(L/L_\odot) = -5.31 \pm 0.12$ dex from the K_s-band magnitude. Our bolometric luminosity estimate using the K_s magnitude agrees with the estimate of $-5.19^{+0.06}_{-0.07}$ dex derived by Wood et al. (2019) based on the absolute K_s magnitude in Crepp et al. (2014) and computed assuming the distance estimated from the HIPPARCOS parallax. The measured bolometric luminosity and mass of HD 19467B are compatible with an age older than ~7 Gyr. These constraints agree with our age estimate. The models of Baraffe et al. (2003) assume solar metallicity, whereas HD 19467B could potentially have slightly subsolar metallicity. Very few evolutionary models explore the effects of metallicity. The models from Saumon & Marley (2008) have a poor sampling (0.3 dex) and assume cloudless atmospheres. The Sonora models (Marley et al. 2017) should soon allow for these issues to be alleviated. However, based on the cloudless models of Saumon & Marley (2008) and assuming linear interpolations, we expect small shifts on the predicted bolometric luminosity and effective temperature toward lower values (~0.03 dex and ~15 K).

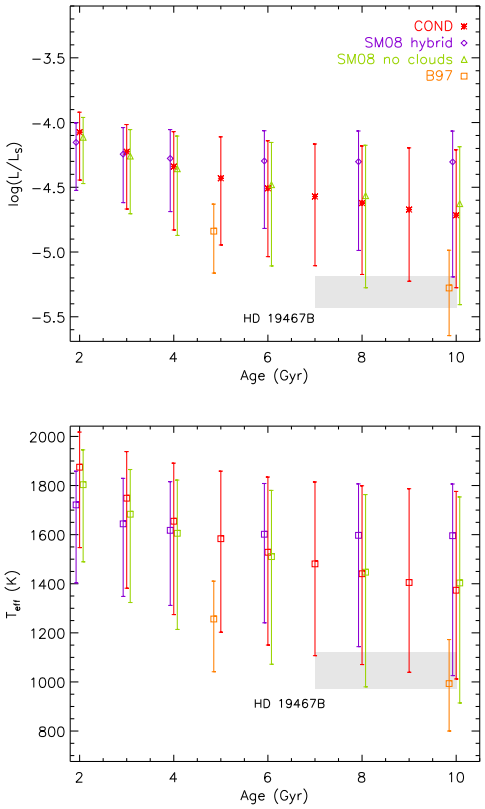

Fig. 16. Bolometric luminosity (*top*) and effective temperature (*bottom*) as a function of the age of HD 19467B (gray area) compared to evolutionary tracks from the models COND (Baraffe et al. 2003), Saumon & Marley (2008) (for two treatments of the clouds), and Burrows et al. (1997) assuming the mass for the companion estimated from the orbital fit and the theoretical hydrogen-burning mass limit (data points). Small horizontal offsets are applied to all models except for COND for clarity.